RESEARCH REPORTS

TIME DEPENDENT VARIATION OF THE STRESS DISTRIBUTION IN A SEMI-INFINITE PLATE COMPRESSED WITH AN ELASTIC FLAT PUNCH

Yoshio OHASHI and Tadashi NISHITANI

Department of Mechanical Engineering

(Received April 12, 1968)

1. Introduction

Problems concerning the compression of a semi-infinite body on a part of its boundary with elastic punch are very important not only in solid mechanics but in engineering practice. They are fundamental problems not only for studying the strength and behavior near the contact part between elements of machine or construction but for estimating the resistance of ground against the building or bridge in the architectural and civil engineerings. Especially, in considering the behavior of a contact part at high temperature or the sinking of ground induced by the structures, it is necessary to take into account creep deformation.

In experimental analyses of such problems, though the stress distribution in an elastic semi-infinite body compressed by a rigid or elastic flat punch on a part of its boundary has been obtained by using the usual photoelasticity, any experiment measuring the change of stress distribution with respect to time has not yet been performed on the creep deformation of semi-infinite body. It seems due to the fact that any suitable experimental method has not yet been developed for such a measurement.

However, in a photo-rheological stress analysis proposed by one of the present authors[1], the stress distribution in a plastically deforming transparent body can be found by analyzing the fringe pattern appearing in the body under polarized light field with the consideration of the instantaneous elasto-plastic strain rate and the creep strain rate. Accordingly, the above mentioned problems may be solved by using this method.

In the present paper, as an example of this method, the stress distribution and its variation with respect to time near the contact surface are investigated experimentally on a semi-infinite plate of softened celluloid compressed on a part of the boundary with a flat punch of araldite which remains in a glassy elastic state.

2. Experimental Apparatus

Fig. 1 shows a schematic diagram of the apparatus used, in which a rectan-

gular celluloid plate kept vertically on a rigid basis is compressed by an araldite flat punch at the central part on its longer side. In order to set the punch correctly on the side of the plate and for reducing the frictional resistance, as shown in the figure, a block carrying the punch is supported by ball bearings around of it. Equal two dead weights are hung at both ends of a rigid bar, and the bar is supported with a knife edge at the center on the upper surface of the block for avoiding the occurance of bending in the block.

To restrict the deformation of the plate in the plane strain state, the plate is arranged under restraint with thick glass plates on both sides of it. Moreover, a vertical movement of the glass plates is permissible because they are supported by ball bearings on their outsides.

When the apparatus is immersed in an oil bath heated at 65°C, the celluloid plate is softened and deforms plastically under external force while the araldite punch is kept in its glassy elastic state. As the mechanical properties of celluloid are sensitive to temperature, variation and non-uniformity of temperature in the specimen are kept within ± 0.05°C with a regulator of thirmister type.

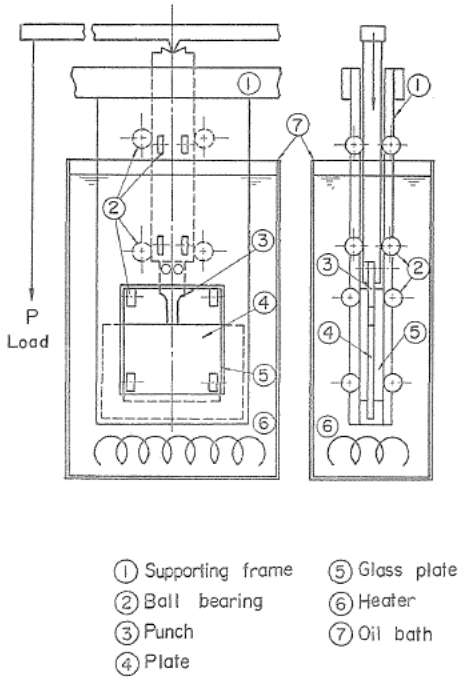

FIG. 1. Experimental apparatus.

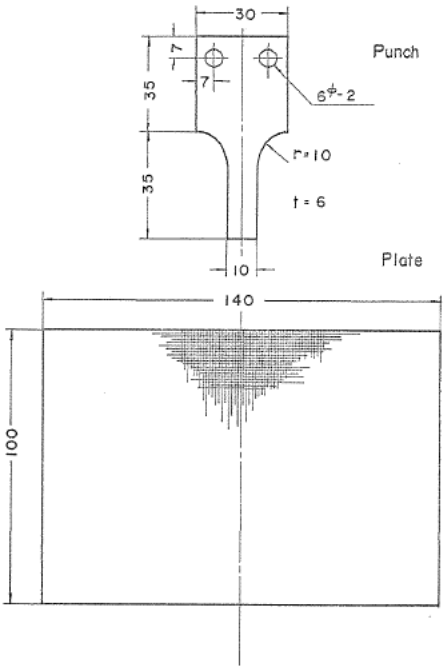

FIG. 2. Geometries of specimens.

3. Specimens

Fig. 2 shows the geometries of the araldite flat punch and the celluloid plate. Though the length of the punch must be long enough lest an effect of stress distribution near the fillet should come to the contact part with the plate, as the punch may bend when it is too long, the length was confined as shown in the figure. The celluloid plate is wide enough to be considered as a semi-infinite plate.

The punch was finished by light cutting with an end-mill from an araldite plate of 6 mm thick without any initial stress, and its contact surface was extremely smooth. The state of araldite at 65°C was examined by a calibration test with two uniaxial tension specimens cut out from the same araldite plate. Fig. 3 shows the result of calibration test. As shown in the figure, the araldite plate was kept in a perfectly glassy elastic state at the temperature, and the fringe stress for the thickness of 6 mm was obtained as $\sigma/N=0.161$ kg/mm^2.

The celluloid plate was prepared from a transparent celluloid plate of 6 mm thick and its contact surface with the punch was also extremely smooth. As shown in the figure, a square network of 1 mm distance was incised on a surface of it for tracing with respect to time the location and state of any assigned point in the

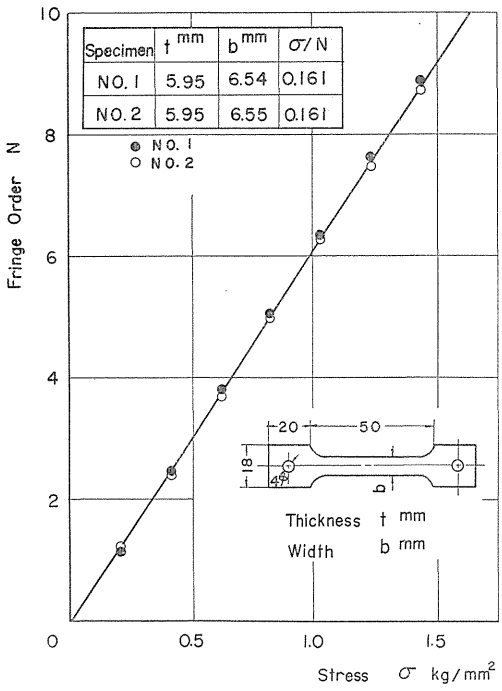

FIG. 3. Result of calibration test of araldite.

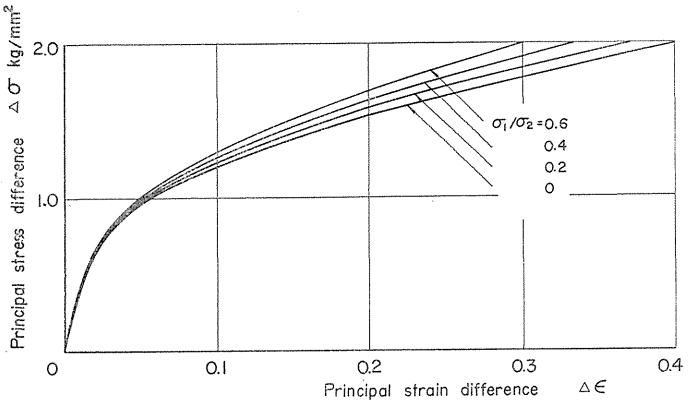

FIG. 4. Relation between $\Delta\sigma$ and $\Delta\varepsilon$ of softened celluloid.

plate after deformation.

According to the method of photo-rheological stress analysis[2], the mechanical properties of the celluloid at 65°C were obtained by a calibration test in which a combined loading of axial compression and hydrostatic pressure was applied to uniaxial compression specimens. The results of the calibration test are shown in Fig. 4. The axial compressive stress and hydrostatic pressure are principal stresses and they are denoted by σ_1 and $\sigma_2=\sigma_3$. The relations between actual

principal stress difference and logarithmic principal strain difference vary in a fairly wide range according to the values of the principal stress ratio σ_1/σ_2 as shown in the figure. In the photo-rheological stress analysis, for the case $\sigma_1 \neq \sigma_2 = \sigma_3$ corresponding to the above mentioned calibration test, the principal strain rate difference $\Delta\dot{\varepsilon}(t)$ is expressed by the next formula,

$$\Delta\dot{\varepsilon}(t) = \frac{2}{\sqrt{3}} B_0 t^{\alpha} \left\{ \frac{\Delta\sigma(t)}{\sqrt{3}} \right\}^{m} + \frac{\Delta\dot{\sigma}(t)}{2G} + \frac{2n+1}{2G} \left\{ \frac{\Delta\sigma(t)}{\sqrt{3}\,k} \right\}^{2n} \Delta\dot{\sigma}(t), \tag{1}$$

and the principal strain difference $\Delta\varepsilon(t)$ is expressed by the next formula obtained by integrating (1) with respect to time,

$$\Delta\varepsilon(t) = \frac{2}{\sqrt{3}} B_0 \int_0^t \tau^{\alpha} \left\{ \frac{\Delta\sigma(\tau)}{\sqrt{3}} \right\}^{m} d\tau + \frac{\Delta\sigma(t)}{2G} \left[1 + \left\{ \frac{\Delta\sigma(t)}{\sqrt{3}\,k} \right\}^{2n} \right]. \tag{2}$$

where $\Delta\sigma(t)$ and $\Delta\dot{\sigma}(t)$ are the principal stress difference and its time rate, and t denotes the time. Values of the coefficients contained in (1) or (2) may be found from the results of calibration test. Fig. 5 shows the result in which the values of the coefficients are shown in relation to the value of σ_1/σ_2. Fig. 6 shows the relation between the principal stress difference and the fringe order per unit thickness obtained by the same calibration test. The relation also varies with the value of σ_1/σ_2 and this is due to the effect introduced from the relation in Fig. 4. According to Fig. 6, the value of fringe order can be expressed as a function of principal stress and strain differences as in the next form:

$$N(t) = 0.21\,\Delta\sigma(t) + 1.1\,\Delta\varepsilon(t) + 0.92\{\Delta\varepsilon(t)\}^{3/2} + 0.1\{\Delta\varepsilon(t)\}^{2}. \tag{3}$$

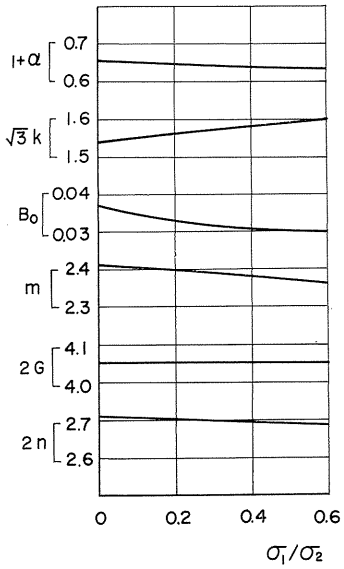

FIG. 5. Values of coefficients.

4. Experimental Procedure and its Result

In the above mentioned apparatus, after the temperature settled as the assigned value, a dead load of 60 kg was applied instantaneously. And the isochromatic and isoclinic fringes were recorded at the instants 2, 40, 160 and 300 min after loading including the isochromatic fringe at the instant of loading. The isochromatic fringe was recorded by photograph through a monochromatic filter of 5461 Å in a circular polarized light field, and the isoclinic pattern was photographed by extinguishing the isochromatic pattern with the use of colour film at a slightly over exposure in a plane polarized light field. The deformed network on the plate also was recorded with them.

Fig. 7 shows the isochromatic fringe photograph at the instant of loading, and Figs. 8 and 9 show the isochromatic fringe photographs at 2 and 300 min after loading. In the photographs at the instant and at 2 min after loading, the

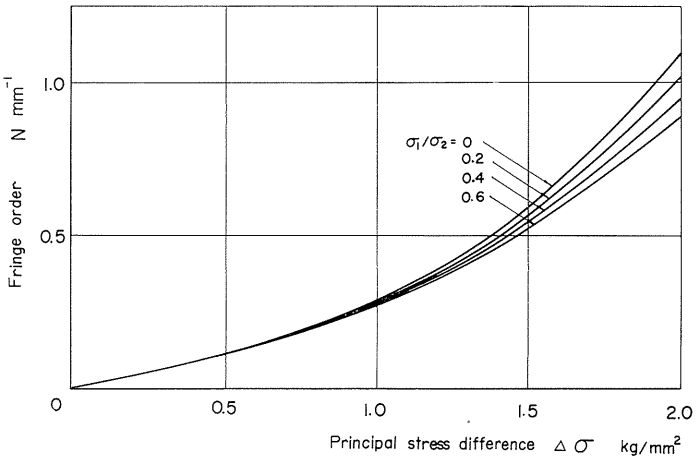

FIG. 6. Relation between fringe order and $\Delta\sigma$.

ranges of uniform compression are visible slightly between the fringes near the fillet and the contact part in the punch. A slight bending appeared in the punch at 300 min after loading. Fig. 10 shows the isoclinic fringe photograph at 2 min after loading and 0° of isoclinic parameter, as an example. Isochromatic and isoclinic patterns are obtained at each instant from these photographs. Fig. 11 is the isochromatic pattern at the instant of loading, and Figs. 12, 13 or Figs. 14, 15 show the isochromatic and isoclinic patterns at 2 or 300 min after loading.

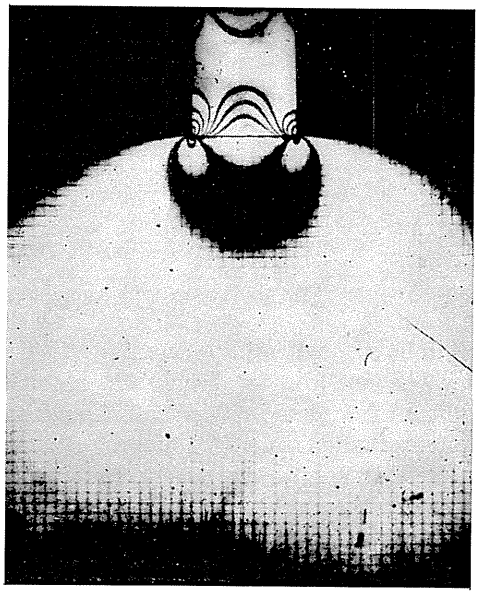

FIG. 7. Isochromatic fringe photograph at the instant of loading.

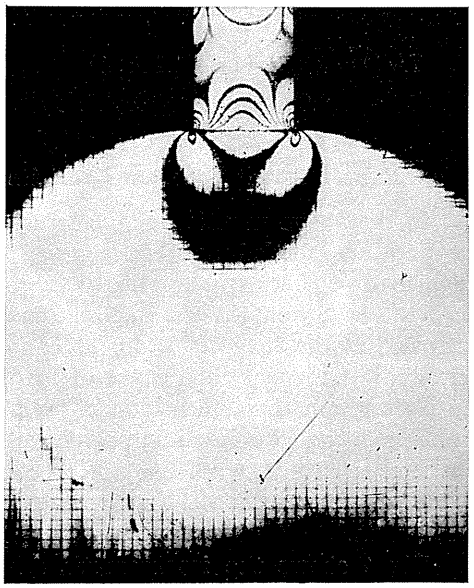

FIG. 8. Isochromatic fringe photograph at 2 min after loading.

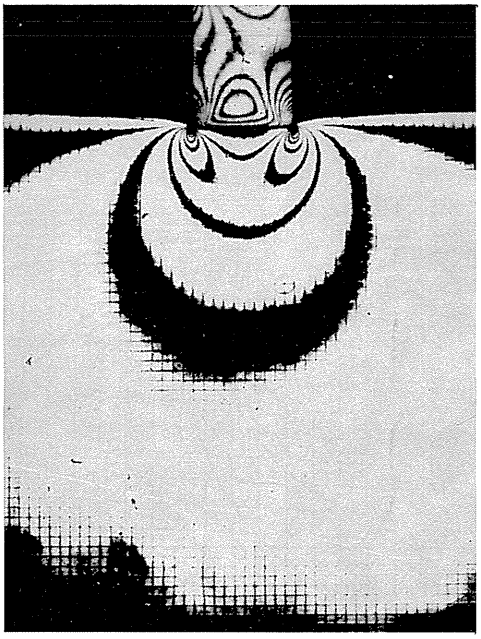

FIG. 9. Isochromatic fringe photograph at 300 min after loading.

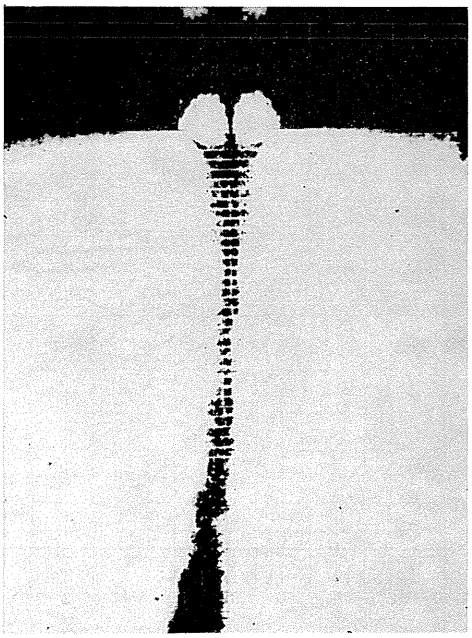

FIG. 10. Isoclinic fringe photograph at 2 min after loading, 0.

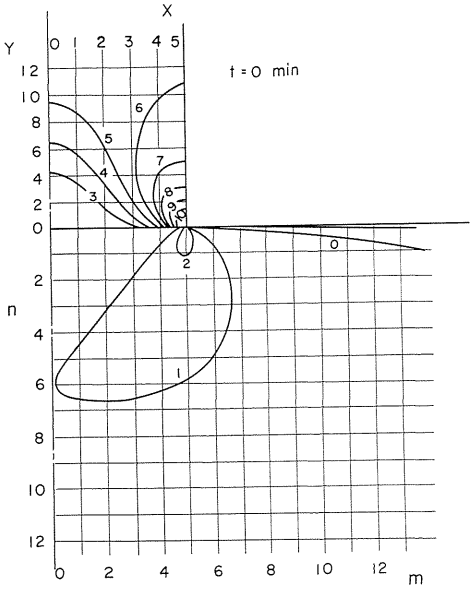

FIG. 11. Isochromatic pattern at the instant of loading.

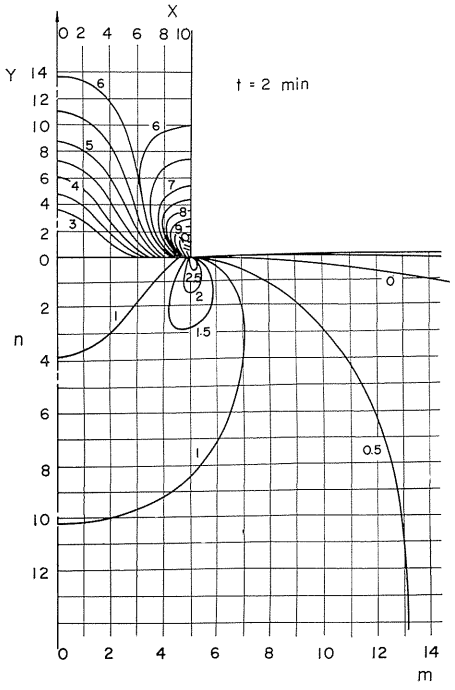

FIG. 12. Isochromatic pattern at 2 min after loading.

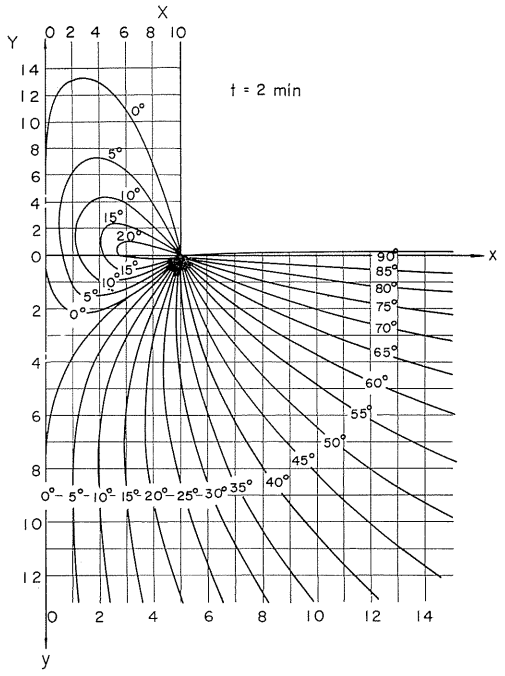

FIG. 13. Isoclinic pattern at 2 min after loading.

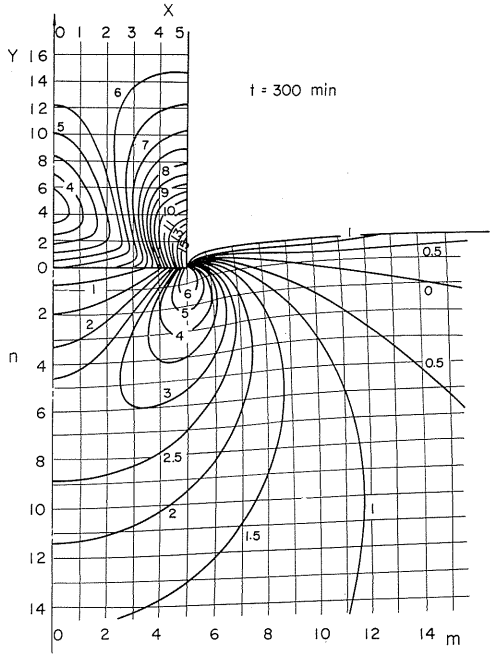

FIG. 14. Isochromatic pattern at 300 min after loading.

5. Analysis of the Principal Stress Difference in the Celluloid Plate

The photo-rheological stress analysis was used for obtaining the distribution of the principal stress difference in the celluloid plate from the isochromatic pattern obtained above. The fundamental relation in the photo-rheological stress analysis under the conditions of plane strain state and incompressibility of material is given as follows[2]:

$$\Delta\dot{\varepsilon}(t) = \frac{B_0}{2^m} t^{\alpha} \left\{ \Delta\sigma(t) \right\}^m + \frac{\Delta\dot{\sigma}(t)}{2G} + \frac{2n+1}{2G} \left\{ \frac{\Delta\sigma(t)}{2k} \right\}^{2n} \Delta\dot{\sigma}(t). \qquad (4)$$

The values of constants contained in the relation have been given as shown in Fig. 5 and they vary with the value of σ_1/σ_2 as shown in the figure. Accordingly, for taking account of these

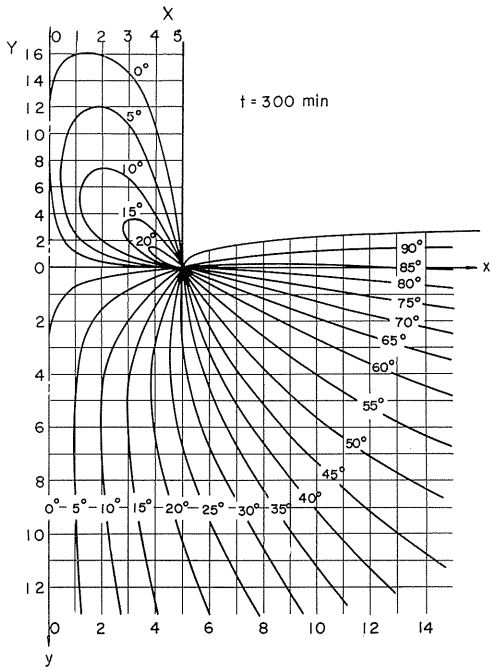

FIG. 15. Isoclinic pattern at 300 min after loading.

variations, it is necessary to know the distribution of the value of σ_1/σ_2. However, as it is impossible in advance, the distribution was approximated as follows. When the case of semi-infinite elastic plate subjected to a uniform load in the corresponding range on its boundary is considered in place of the compression with punch, the distribution of the values of σ_1/σ_2 has been obtained theoretically as shown in Fig. 16. If we assume that the value of σ_1/σ_2 at each point on the deformed celluloid plate may be replaced with the values shown in Fig. 16, the value of σ_1/σ_2 at each node of the network may be obtained by the linear interpolation as the value of σ_1/σ_2 at the point in Fig. 16 corresponding to the location of this node. Then, the values of constants at each node of the deformed network may be found from Fig. 5 according to the value of σ_1/σ_2 obtained above.

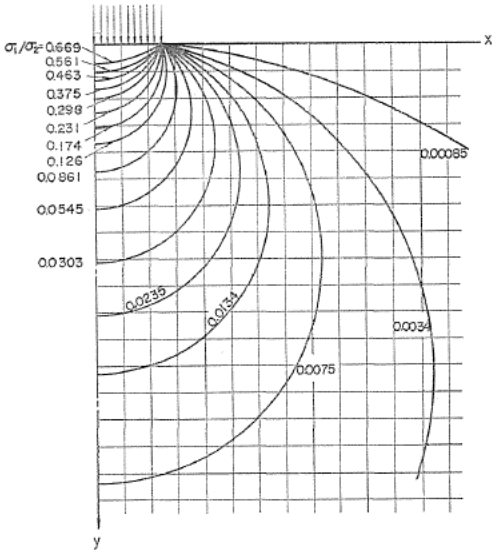

FIG. 16. Distribution of σ_1/σ_2 in an elastic plate under partial uniform compression.

The value of the fringe order at each node in the deformed network may be found as follows. As shown in Fig. 9, for example, the vertical and horizontal lines in the deformed network are denoted as $m=0, 1, 2, \ldots$ and $n=0, 1, 2, \ldots$. These lines become curves after deformation and the lengths between each node of them are not always equal with each other. Therefore, by denoting the vertical and horizontal distances between two adjucent nodes with Δx and Δy, the length between these two nodes was calculated by using a formula $\{(\Delta x)^2+(\Delta y)^2\}^{1/2}$. Then, the length of each curve was found by summing up these amounts. The distances Δx and Δy were measured by a micrometer with accuracy of 0.005 mm under magnifying projector from the photograph of deformed network. The location of intersection of the curve with the isochromatic fringe was measured also in the same manner. As the result of the procedure, distribution curves of the fringe order along the vertical and horizontal curves may be found. Fig. 17 and 18 show the distribution curves of fringe order along the curves $m=4$ and $n=7$, respectively. In these curves, the fringe order corresponding to each node may be obtained. The values of fringe order corresponding to the same node obtained from the curves $m=$const and $n=$const agree well with each other. In such a way, finding the fringe orders at each node in series of instants and describing them in diagrams, the variation of the fringe order with respect to time was found in the element corresponding to any node. Fig. 19 shows an example of such diagrams. Accordingly, the slope of the tangent to the curve corresponds to the next formula obtained by differentiating (3):

$$\dot{N}(t) = 0.21\,\Delta\dot{\sigma}(t) + 1.1\,\Delta\dot{\varepsilon}(t) + [1.38\{\Delta\varepsilon(t)^{1/2} + 0.2\,\Delta\varepsilon(t)\}]\Delta\dot{\varepsilon}(t). \tag{5}$$

The value of $\Delta\varepsilon(t)$ contained in (5) must be found by integrating (4) with respect

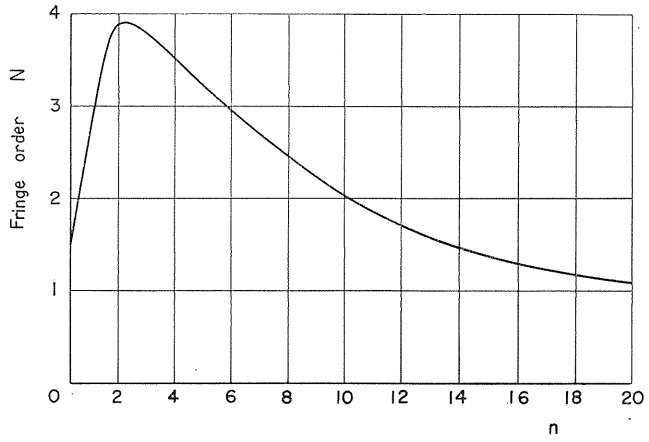

FIG. 17. Distribution of fringe order along Curve $m=4$.

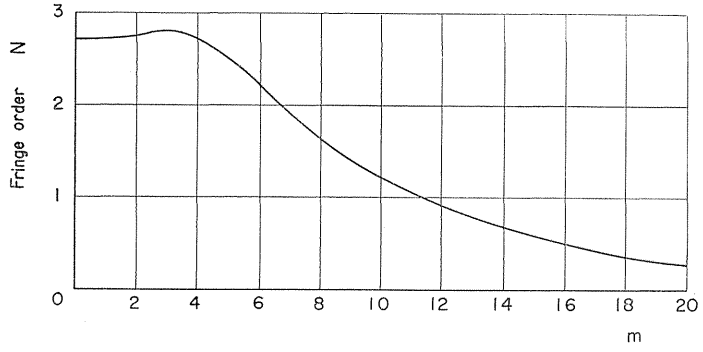

FIG. 18. Distribution of fringe order along Curve $n=7$.

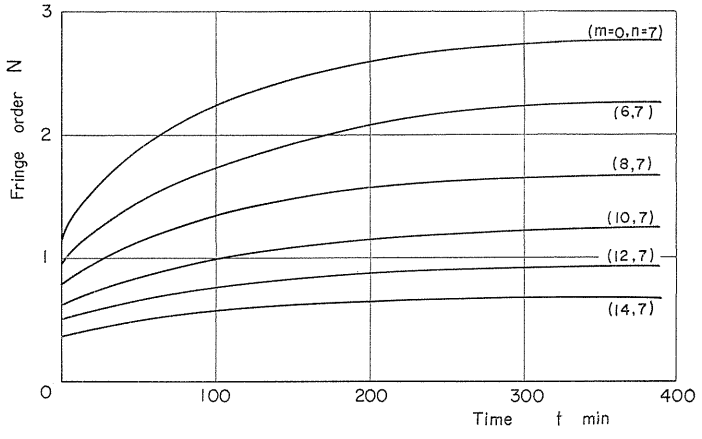

FIG. 19. Variations of fringe order with repect to time at several nodes.

to time, and in the integration, it is necessary to assume that the directions of the principal stress and strain in the element are parallel to the path of the element through deformation. Integrating (4) under such condition, the next relation is obtained:

$$\Delta\varepsilon = \frac{B_0}{2^m}\int_0^t \tau^\alpha \{\Delta\sigma(\tau)\}^m d\tau + \frac{\Delta\sigma(t)}{2G}\left[1 + \left\{\frac{\Delta\sigma(t)}{2k}\right\}^{2n}\right]. \tag{6}$$

As the concrete form of the function under the integral sign can not be found in advance, the integral term is estimated as follows. Subdividing the time into small intervals in which the magnitude of $\Delta\dot{\sigma}(t)$ may be considered as constant; $0\sim t_1$, $t_1\sim t_2$, ..., $t_n\sim t_{n+1}$, the integral term in (6) can be expressed for interval $t_n\sim t_{n+1}$ as follows:

$$\int_{t_n}^{t_{n+1}} \tau^\alpha \{\Delta\sigma(t_n) + \Delta\dot{\sigma}(t_n)(\tau - t_n)\}^m d\tau.$$

Accordingly, expressing the integral term in the next form;

$$\int_0^{t_{n+1}} \tau^\alpha \{\Delta\sigma(\tau)\}^m d\tau = \int_0^{t_n} \tau^\alpha \{\Delta\sigma(\tau)\}^m d\tau + \int_{t_n}^{t_{n+1}} \tau^\alpha \{\Delta\sigma(t_n) + \Delta\dot{\sigma}(t_n)(\tau - t_n)\}^m d\tau,$$

we assume that the first term has been found by the procedure and that the second term will be found by the same way. Expanding into series and integrating by term, the second term of the right hand side of the above expression becomes as follows:

$$\begin{aligned}\int_{t_n}^{t_{n+1}} \tau^\alpha \{\Delta\sigma(t_n) + \Delta\dot{\sigma}(t_n)(\tau - t_n)\}^m d\tau &= \Delta\dot{\sigma}(t_n)^m \frac{t_{n+1}^{\alpha+m+1} - t_n^{\alpha+m+1}}{\alpha+m+1} + m\Delta\dot{\sigma}(t_n)^{m-1} \\ &\times \{\Delta\sigma(t_n) - \Delta\dot{\sigma}(t_n)t_n\}\frac{t_{n+1}^{\alpha+m} - t_n^{\alpha+m}}{\alpha+m} + \frac{m(m-1)}{2!}\Delta\dot{\sigma}(t_n)^{m-2}\{\Delta\sigma(t_n) - \Delta\dot{\sigma}(t_n)t_n\}^2 \\ &\times \frac{t_{n+1}^{\alpha+m-1} - t_n^{\alpha+m-1}}{\alpha+m-1} \\ &+ \frac{m(m-1)(m-2)}{3!}\Delta\dot{\sigma}(t_n)^{m-3}\{\Delta\sigma(t_n) - \Delta\dot{\sigma}(t_n)t_n\}^3 \frac{t_{n+1}^{\alpha+m-2} - t_n^{\alpha+m-2}}{\alpha+m-2} + \cdots.\end{aligned}$$

Therefore, (6) becomes as follows:

$$\begin{aligned}\Delta\varepsilon(t) = \frac{B_0}{2^m}\Bigg[&\int_0^{t_n} \tau^\alpha \{\Delta\sigma(\tau)^m d\tau + \Delta\dot{\sigma}(t_n)^m \frac{t_{n+1}^{\alpha+m-1} - t_n^{\alpha+m-1}}{\alpha+m-1} + m\Delta\dot{\sigma}(t_n)^{m-1} \\ &\times \{\Delta\sigma(t_n) - \Delta\dot{\sigma}(t_n)t_n\}\frac{t_{n+1}^{\alpha+m} - t_n^{\alpha+m}}{\alpha+m} + \frac{m(m-1)}{2!}\Delta\dot{\sigma}(t_n)^{m-2} \\ &\times \{\Delta\sigma(t_n) - \Delta\dot{\sigma}(t_n)t_n\}^2 \frac{t_{n+1}^{\alpha+m-1} - t_n^{\alpha+m-1}}{\alpha+m-1} + \cdots\Bigg] + \frac{\Delta\sigma(t)}{2G}\left[1 + \left\{\frac{\Delta\sigma(t)}{2k}\right\}^{2n}\right].\end{aligned} \tag{7}$$

The above expression has a good convergency.

Assigning an instant of loading as $t=t_0=0$, the isochromatic fringe pattern corresponding to the instant is shown in Fig. 11, and the fringe order corresponds to the next formula:

$$N(t_0) = 0.21\,\Delta\sigma(t_0) + 1.1\,\Delta\varepsilon(t_0) + 0.92\{\Delta\varepsilon(t_0)\}^{3/2} + 0.1\{\Delta\varepsilon(t_0)\}^2. \tag{8}$$

For $t=t_0=0$, the value of $\Delta\varepsilon(t_0)$ becomes as in the next form obtained from (6):

$$\Delta\varepsilon(t_0)=\frac{\Delta\sigma(t_0)}{2G}\left[1+\left\{\frac{\Delta\sigma(t_0)}{2k}\right\}^{2n}\right]. \tag{9}$$

Solving an equation obtained by substituting (9) into (8) with the value of $N(t_0)$ corresponding to each node, the value of $\Delta\sigma(t_0)$ may be found at each node. The value of $\Delta\varepsilon(t_0)$ may be found by substituting the just obtained value into (9). The value of $\Delta\dot{\varepsilon}(t_0)$ and $\dot{N}(t_0)$ can be expressed from (4) and (5) as follows;

$$\Delta\dot{\varepsilon}(t_0)=\frac{\Delta\dot{\sigma}(t_0)}{2G}+\frac{2n+1}{2G}\left\{\frac{\Delta\sigma(t_0)}{2k}\right\}^{2n}\Delta\dot{\sigma}(t_0), \tag{10}$$

$$\dot{N}(t_0)=0.21\,\Delta\dot{\sigma}(t_0)+1.1\,\Delta\dot{\varepsilon}(t_0)+[1.38\{\Delta\varepsilon(t_0)\}^{1/2}+0.2\,\Delta\varepsilon(t_0)]\Delta\dot{\varepsilon}(t_0), \tag{11}$$

respectively. As the values of $\Delta\sigma(t_0)$ and $\Delta\varepsilon(t_0)$ in (10) and (11) have been obtained above and the value of $\dot{N}(t_0)$ may be found from the result of experiment, the value of $\Delta\dot{\sigma}(t_0)$ may be found from (10) and (11). Then, at the last time t_1 of the corresponding interval, the value of $\Delta\sigma(t_1)$ may be found from the next relation:

$$\Delta\sigma(t_1)=\Delta\sigma(t_0)+\Delta\dot{\sigma}(t_0)(t_1-t_0)=\Delta\sigma(t_0)+t_1\Delta\dot{\sigma}(t_0). \tag{12}$$

For the next interval $t_1\sim t_2$, the value of $\Delta\varepsilon(t_1)$ may be obtained by the next relation corresponding to (7):

$$\Delta\varepsilon(t_1)=\frac{B_0}{2^m}\left[\left\{\Delta\dot{\sigma}(t_0)\right\}^m\frac{t_1^{\alpha+m+1}}{\alpha+m+1}+m\{\Delta\dot{\sigma}(t_0)\}^{m-1}\Delta\sigma(t_0)\frac{t_1^{\alpha+m}}{\alpha+m}\right.$$
$$\left.+\frac{m(m-1)}{2!}\{\Delta\dot{\sigma}(t_0)\}^{m-2}\{\Delta\sigma(t_0)\}^2\frac{t^{\alpha+m-1}}{\alpha+m-1}+\cdots\right]+\frac{\Delta\sigma(t_1)}{2G}\left[1+\left\{\frac{\Delta\sigma(t_1)}{2k}\right\}^{2n}\right]. \tag{13}$$

And the value of $\Delta\dot{\varepsilon}(t_1)$ is found by the next relation corresponding to (4):

$$\Delta\dot{\varepsilon}(t_1)=\frac{B_0}{2^m}t_1^{\alpha}\{\Delta\sigma(t_1)\}^m+\frac{\Delta\dot{\sigma}(t_1)}{2G}\left[1+(2n+1)\left\{\frac{\Delta\sigma(t_1)}{2k}\right\}^{2n}\right]. \tag{14}$$

By substituting (12), (13) and (14) into (5), the relation between $\dot{N}(t_1)$ and $\Delta\dot{\sigma}(t_1)$ may be found. As the value of $\dot{N}(t_1)$ at each node may be found from Fig. 19, the value of $\Delta\dot{\sigma}(t_1)$ may be obtained from the last relation. Therefore, at the last time t_2 of the corresponding interval to $\Delta\dot{\sigma}(t_1)$, the value of $\Delta\sigma(t_2)$ can be found from the next relation:

$$\Delta\sigma(t_2)=\Delta\sigma(t_1)+\Delta\dot{\sigma}(t_1)(t_2-t_1). \tag{15}$$

The value of $\Delta\varepsilon(t_2)$ can be obtained from the next relation corresponding to (7):

$$\Delta\varepsilon(t_2)=\frac{B_0}{2^m}\left[\int_0^{t_1}\tau^{\alpha}\{\Delta\sigma(\tau)\}^m d\tau+\{\Delta\dot{\sigma}(t_1)\}^m\frac{t_2^{\alpha+m+1}-t_1^{\alpha+m+1}}{\alpha+m+1}\right.$$
$$\left.+m\{\Delta\dot{\sigma}(t_1)\}^{m-1}\{\Delta\sigma(t_1)-\Delta\dot{\sigma}(t_1)t_1\}\frac{t_2^{\alpha+m}-t_1^{\alpha+m}}{\alpha+m}+\cdots\right]+\frac{\Delta\sigma(t_2)}{2G}\left[1+\left\{\frac{\Delta\sigma(t_2)}{2k}\right]^{2n}\right\}. \tag{16}$$

The integral term in the above relation, as it is easily seen, corresponds to the expression in the first bracket of the right hand side of (13). The value of $\Delta\dot{\varepsilon}(t_2)$ can be found from the next relation corresponding to (4):

$$\Delta\dot{\varepsilon}(t_2)=\frac{B_0}{2^n}t_2^a\{\Delta\sigma(t_2)\}^m+\frac{\Delta\dot{\sigma}(t_2)}{2G}\left[1+(2n+1)\left\{\frac{\Delta\sigma(t_2)}{2k}\right\}^{2n}\right]. \tag{17}$$

By substituting (15), (16) and (17) into (5), the relations between $\Delta\dot{\sigma}(t_2)$ and $\dot{N}(t_2)$ is obtained. Therefore, the value of $\Delta\dot{\sigma}(t_2)$ can be found from the last relation by using the value of $\dot{N}(t)_2$ found from Fig. 19 at each node at the instant t_2. As the values of constants in the relations in the above mentioned calculations

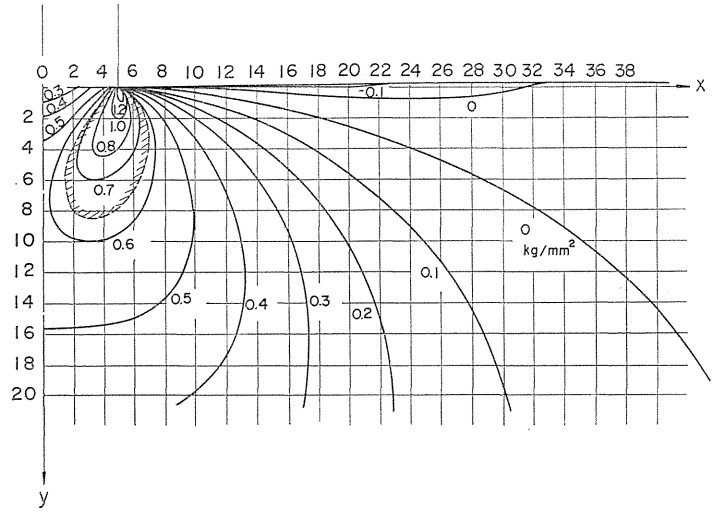

FIG. 20. Distribution of $\Delta\sigma$ in the plate at 2 min after loading.

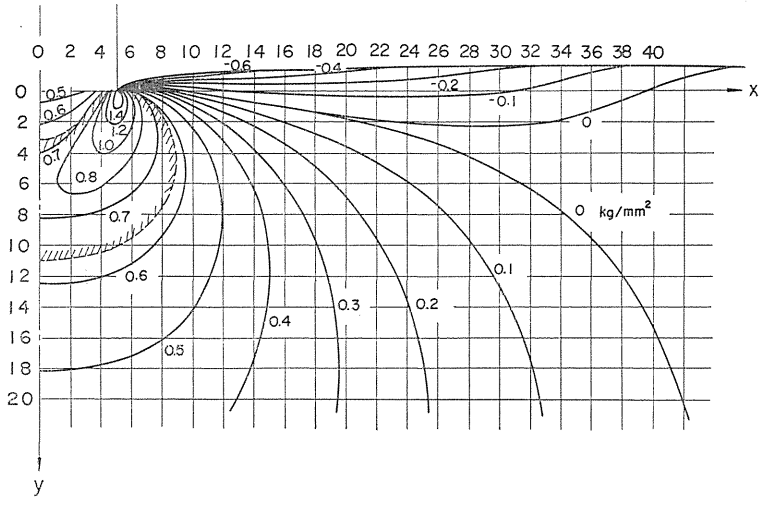

FIG. 21. Distribution of $\Delta\sigma$ in the plate at 300 min after loading.

vary with the value of σ_1/σ_2 as mentioned above, it is necessary to use the values corresponding to each node obtained from Fig. 5 in refering Fig. 16 for each node. In the same manner, the values of $\Delta\sigma(t)$ for all nodes may be found for each instant. The above mentioned calculation were performed by an electronic computer for several time increments: 1 min for 0~6 min, 2 min for 6~20 min, 5 min for 20~100 min, 10 min for 100~200 min, 20 min for 200~360 min.

As the result of the calculation, the values of $\Delta\sigma(t)$, $\Delta\varepsilon(t)$ and $\Delta\dot{\varepsilon}(t)$ for all of nodes were obtained. However, as the instant when the location of the node in the plate were measured are the instants $t=0$, 2, 40, 160 and 300 min, the distribution of $\Delta\sigma(t)$ in the plate can be obtained only for these instants. Figs. 20 and 21 show the distribution of $\Delta\sigma$ in the plate at 2 and 300 min after loading for example.

6. Stress Distribution in the Punch

As the material of the punch remains in the elastic state, the stress distribution in the punch may be found by using the ordinary photoelasticity. For example, they are found by the shear difference method from the isochromatic and isoclinic patterns obtained by the experiment at 2 min after loading shown in Figs. 12 and 13. As shown in these figures, a cartesian coordinate systems X Y, in which Sections $X=0$, 1, ..., 10 divide the half width of the punch equally and Sections $Y=0$, 1, 2, ... are entered in the same distance, is described on the pattern of the punch. Figs. 22 and 23 show the distributions of stress components within the punch at 2 and 300 min after loading.

In these figures, the value of τ_{xy} was obtained directly from the fringe order

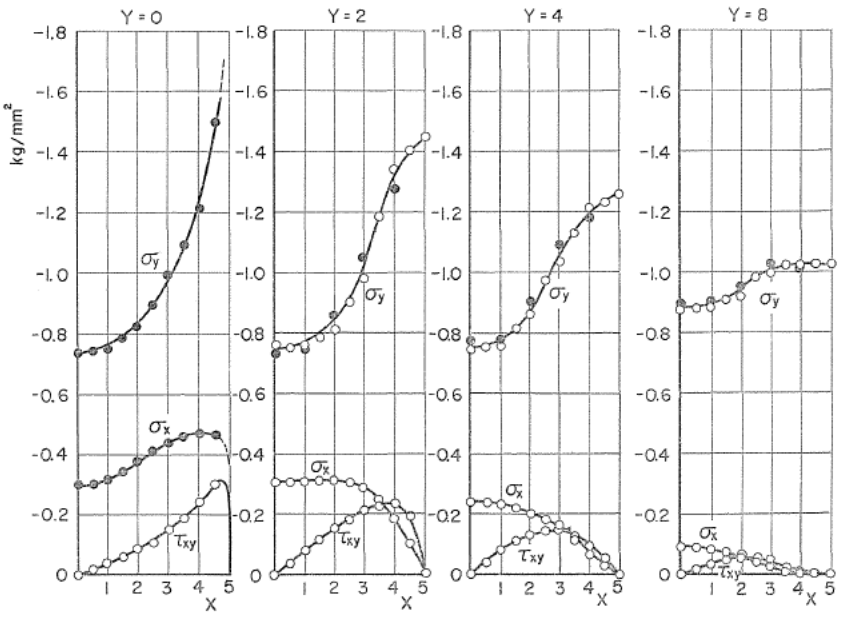

FIG. 22. Distribution of stress components in the punch at 2 min after loading.

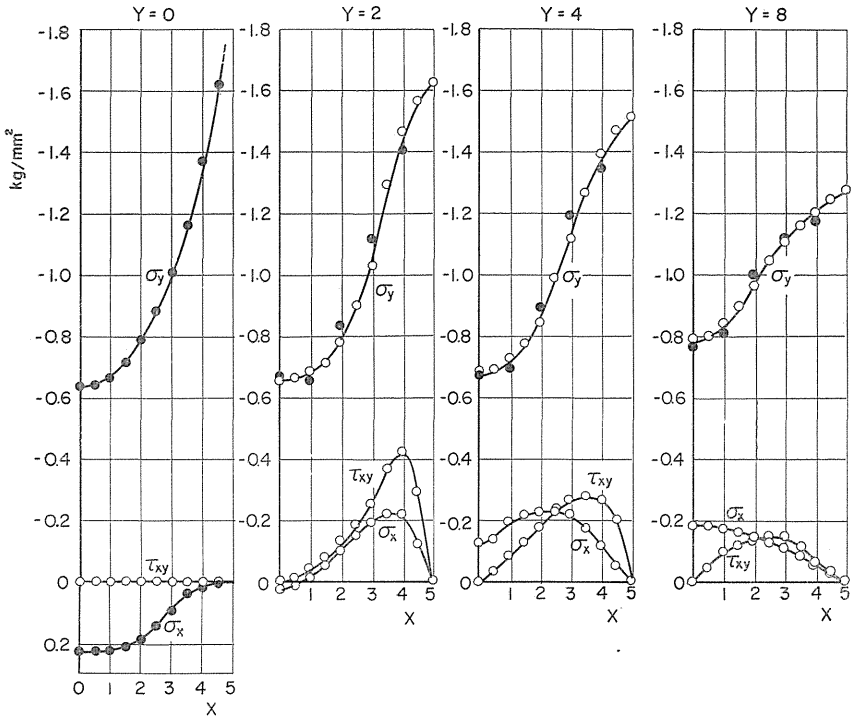

FIG. 23. Distributions of stress components in the punch at 300 min after loading.

and isoclinic parameter on each node, and the values of σ_x and σ_y shown with open ciecles were found by the shear difference method along the sections parallel to X-axis beginning from the free surface, and those shown with solid circles were obtained by the same method in the Y-direction according to the distribution on Section $Y=16$ obtained in the X-direction by this method. The corresponding values shown with open and solid circles on Sections $Y=2$, 4 and 8 agree well in each figure. As Section $Y=0$ in each figure is a contact surface and the values cannot be obtained in the X-direction, only the values shown with solid circles, obtained in the Y-direction, are entered.

7. Stress Distribution in the Celluloid Plate

According to the experimental result obtained by Frocht and Cheng[3], isoclinic parameters in the plastically deformed celluloid represent the directions of the principal stress regardless of the state of material, the state of stress and its history. Then, the stress components in the plate may be obtained by the shear difference method from the isoclinic pattern obtained by the experiment and the distribution of the principal stress differences found by the photo-rheological stress analysis.

For example, as shown in Figs. 13 and 20, a cartesian coordinate system $x\,y$, in which Sections $x=0$, 1, 2, ... are entered in the distance dividing the half width of the punch into equal 5 parts and Sections $y=0$, 1, 2, ... are entered in the same distance, is considered in the plate. As the stress components under the contact

surface cannot be obtained directly by the shear difference method, Section $x=7$ is selected first as a basis. In Section $x=7$, the free surface lies on the minus side of y. As the values of σ_x and σ_y on the surface may be found from the value of principal stress obtained from Fig. 20 and inclination of the surface, the values of σ_x and σ_y on the section were found by the shear difference method performed in the y-direction using the stress values on the surface as the boundary values.

The values of stress components at almost of other nodes were obtained by the shear difference method performed in the x-direction starting from this section. However, as the point of $x=5$ and $y=0$ is a singular point of stress distribution and the numerical integration cannot be performed through this point, in the part near the contact surface, the stress distribution were obtained by performing

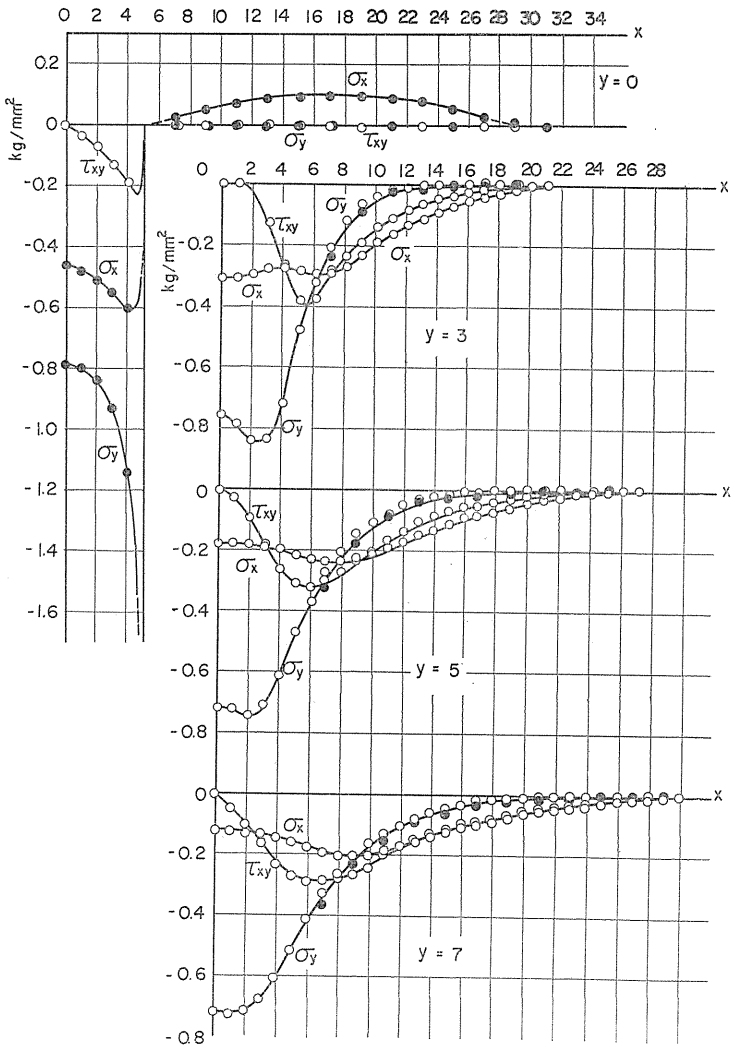

FIG. 24. Distributions of stress components in the plate at 2 min after loading.

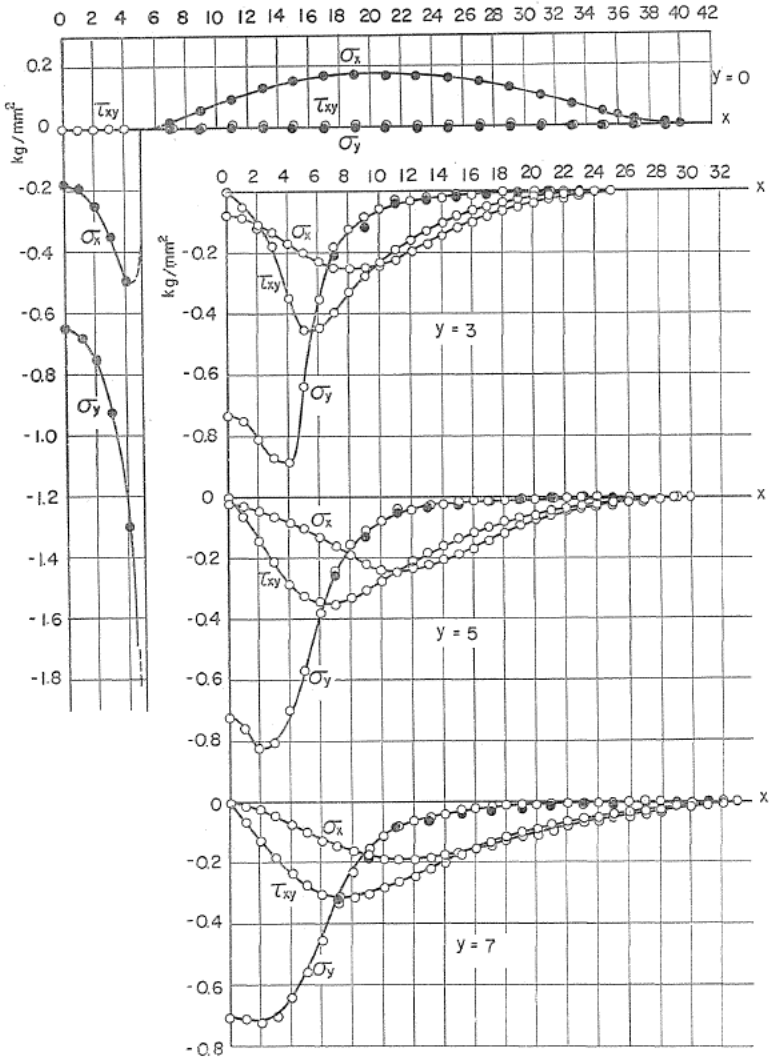

FIG. 25. Distributions of stress components in the plate at 300 min after loading.

the numerical integration in the y-direction according to the stress values on Section $y=3$.

Figs. 24 and 25 show the distributions of stress components at 2 and 300 min after loading, respectively. In these figures, the value of τ_{xy} can be found directly without numerical integration. The solid circles on Section $y=0$ show the values obtained by numerical integration performed in the y-direction from the free surface in the range $x>7$ and the values on the contact surface obtained by the above mentioned procedure. On Sections $y=3$, 5 and 7, the values of σ_x and σ_y entered with open circles show the values obtained in the x-direction according to the values on Section $x=7$. The values of σ_y entered with solid circles on Sections $x=7$, 9, 11, ... show the values obtained in the y-direction directly from the free surface and agree well with the corresponding open circles.

8. Stress Distribution on the Contact Surface

Fig. 26 shows the stress distributions at the four instants mentioned above in which the distributions on the punch and plate sides correspond to the solid and open circles, respectively. As shown in the figure, the corresponding values of σ_y on both sides of the contact surface obtained by the different method independently agree well with each other at each instant, and the condition of continuity of the normal stress component on the contact surface is satisfied well.

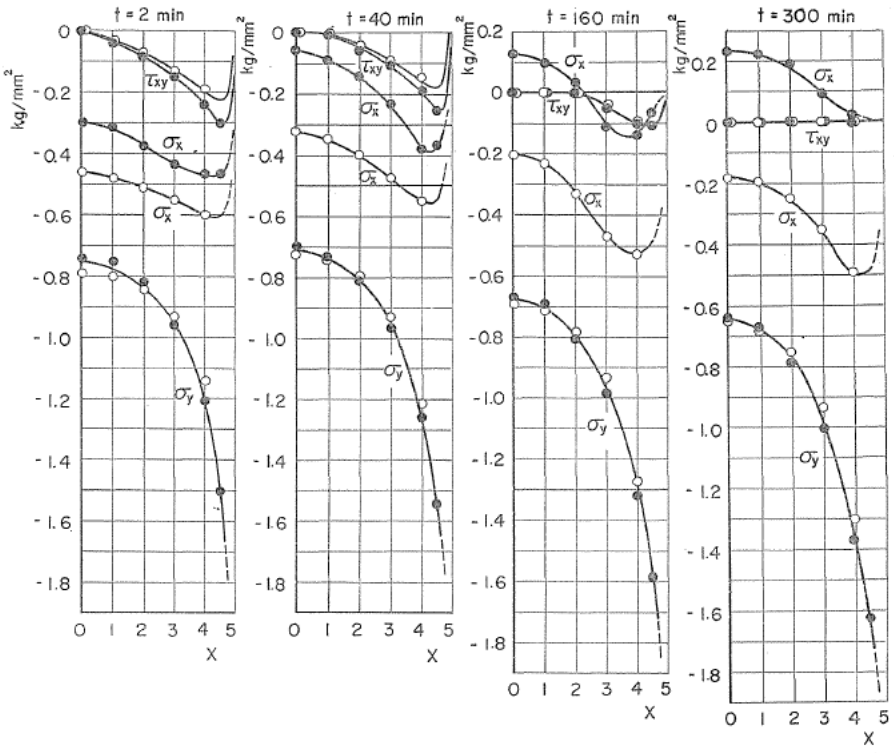

FIG. 26. Stress distribution on the contact surface.

The variation of the distribution of shear stress with respect to time on the contact surface is very interesting as an indication of a settling process of the punch on the plate. At 2 min after loading, the value of shear stress has the maximum values amount to about 25 percent of the mean compressive stress near the ends of contact surface.

When the punch is pressed against the plate, the punch tries to expand towards the both sides of the contact surface. However, as the expansion is constrained by the friction which occurs from the contact with the plate, which cannot deform at once because of the restriction from the parts extending infinitely to both sides of the contact parts, the shear stresses as shown in Fig. 27 occur on both surfaces of contact and these values become larger towards both ends with the value of contact pressure. The reason why the value on the punch side is larger than that on the plate side may be considered as follows. The oil film

lying between both surfaces of contact is squeezed and moves from both end where the contact pressure is higher towards the central part where the pressure is lower. Therefore, the frictional stress between oil film and surface is added to the above mentioned shear stress on the punch side while it is subtracted from the shear stress on the plate side.

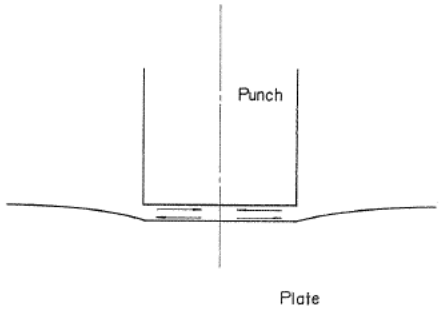

FIG. 27. Directions of shear stresses acting on both surfaces of contact.

At 40 min after loading, in a narrow range of the central part of the contact surface, the shear stress between punch and plate has vanished due to the deformation of the plate. Such a range without shear stress spreads as far as 40 percent of contact surface at 160 min after loading and the difference between the shear stresses on both surfaces in the rest of contact surface has vanished, which snows that the movement of oil film has been completed. Moreover, at 300 min after loading, the shear stress on the contact surface has vanished completely. This may show that the plate has finished the deformation and the punch has settled on the contact surface.

The variation of the distribution of σ_x with respect to time on the contact surface also corresponds to the above mentioned process. The difference between the corresponding two curves of σ_x on the contact surface, which is the component tangential to the surface, is possible because each component may be equilibrated independently from each other on the contact surface. As shown in the figure, these differences at the four instants are almost constant along the contact surface. This fact may be explained by the reason that the plate under contact surface is constrained by the parts of the plate extending to both sides of the contact surface.

At 2 min after loading, as the lateral expansion of the punch compressed vertically is constrained by the plate on the contact surface, the value of σ_x on the surface of the punch appears as a compressive stress. While the deformation in the lateral direction of the plate is restricted by the parts of plate extending to both sides which still remain in undeformed state, and the stress σ_x in the plate on the contact surface appears as a compressive one larger than that in the punch. With a lapse of time, the deformation is transmitted gradually towards the parts extending to both sides, and the constraint against the part just under the contact surface may be reduced. Then, the compressive stress σ_x just under the contact surface also decreases with the deformation of the plate towards the both sides.

The compressive stress σ_x in the punch decreases more remarkably with the deformation of the plate, and at 160 min after loading, it turns into a tensile stress in the central part where the shear stress has vanished. At 300 min after loading, the compressive stress in the plate decreases a little more while the value of σ_x on the punch side turns into a tensile stress along the contact surface.

9. Discussion and Conclusion

As shown in the above figures describing the stress distribution, the corre-

sponding values at the same point obtained by the numerical integration along the different pathes agree well, and the accuracy of the results obtained by the shear difference method may be considered to be sufficiently high. In Fig. 26, the contact pressure on the surface obtained by the quite different methods independently agree almost perfectly. In the figure, mean values of σ_y and the experimental value of mean compressive stress -1.0 kg/mm^2 agree with each other within 3 percent of error. From the above discussion, the results obtained above have a sufficient accuracy, and the validity and high accuracy of the applied method have been proved.

From the results obtained, the process of deformation with lapse of time may be summarized as follows:

1. At the instant of loading, the pressure on the contact surface has very large values at both ends of it and has a minimum at the center of the surface. The value of σ_x on the contact surface of the punch is compressive, and that on the side of the plate is the larger compressive stress due to the constraint of the outer parts of the plate. In the early stage of deformation, there is a slight difference between the corresponding distributions of shear stress on both sides of the contact surface, which may be attributed to the behavior of the oil film being squeezed between both surfaces.

2. At 2 min after loading, with the distance from the contact surface, the stress components σ_x and τ_{xy} vanish gradually and the component σ_y is averaged in the punch. In the plate, however, the shear stress near both ends of the contact surface increases first quickly towards the inside of the plate and decreases gradually thereafter. The values of σ_x and σ_y decrease towards the inside of the plate.

3. With a lapse of time, the value of σ_y in the plate tends to concentrate under the contact surface, on the contrary, the value of σ_x decreases under the contact surface while it increases on both sides. The shear stress on the contact surface disappears gradually from the central part to both ends and it vanishes perfectly at 300 min after loading. On the other hand, the shear stress in the plate quickly increases towards the inside in a certain range under both ends of the contact surface and propagates also in the lateral direction. The value of σ_x on the contact surface of the punch decreases first and turns into a tensile stress. However, at 300 min after loading, along Section $Y=2$ in the punch, σ_x is a compressive stress and the large value of shear stress appears. In such a way, in the punch, the disturbance in the stress distribution propagates from the contact surface with a lapse of time.

The values of principal stress difference corresponding to the equivalent stress to which the equivalent residual strain is 0.2 percent can be obtained from Fig. 4 as $\Delta\sigma=0.624$ kg/mm^2 for $\sigma_1/\sigma_2=0$ and $\Delta\sigma=0.7$ kg/mm^2 for $\sigma_1/\sigma_2=0.6$. Assuming that these values may correspond to the yield stress of the plate, the plastic regions in the plate correspond to the areas surrounded by the dashed curves with shaded line in Figs. 20 and 21. In these figures, it is easily seen that the plastic regions appearing first near by the both ends of the contact surface expand and join together with lapse of time.

Though the above estimation of yield stress might be inadequate in refering the curves shown in Fig. 4, if we approximate the material as a rigid-perfect plastic one, the plastic regions near the both ends of contact surface con-

strained individually first by the rigid part, which cannot show any large plastic deformation, expand with time and join together. At this stage, the rigid part of the plate under the surface joins with the punch and they are supported on the plastic region in the hollow of the other rigid part of the plate. Such state may show a large plastic deformation.

The reason why the stress varies with respect to time near by the contact surface while the compressive load remains constant is consists in the fact that the deformation of the plate is of a transient period. As shown in Fig. 20, at 2 min after loading, the deformation of the plate remains comparatively small region and the intensity of tensile stress on the free surface of the plate remains comparatively small. However, the deformed region and the intensity of tensile stress on the surface gradually increase with time, and these magnitudes attain to the state as shown in Fig. 21 at 300 min after loading. In the figure, a remarkable change appears in the surface layers on both sides of the contact surface in addition to the part under the contact surface. The stress distribution in the plate is kept almost invariably after 300 min.

References

1) Y. Ohashi, Kikai no Kenkyu, **12** (1960), No. 11, 1433 (in Japanese), Brit. J. Appl. Phys., **16** (1965), 985.
2) Y. Ohashi and T Nishitani, Bulletin of JSME, **9** (1966), No. 34, 245, **10** (1967), No. 39, 456.
3) M. M. Frocht and Y. F. Cheng, J. Appl. Mech., Trans. ASME, Ser. E, **29** (1962), No. 1, 1.